# Adiabatic Passage Through Level Anti-Crossings in Systems of Chemically Inequivalent Protons Incorporating Parahydrogen: Theory, Experiment, and Prospective Applications

[1]Maria-Jose Ferrer, Erin Louise Kuker,[2] Evgeniya Semenova,[1] Anghelo J. Gangano,[1] Michelle P. Lapak,[1] Alexander J. Grenning,[1] Vy M. Dong,[2] and Clifford R. Bowers[1,3,*]

[1]Department of Chemistry, University of Florida, Gainesville, FL 32611-7200, USA
[2]Department of Chemistry, University of California, Irvine, CA, 92697-2025, USA
[3]National High Magnetic Field Lab, Tallahassee, FL, 32310, USA

*KEYWORDS: Hyperpolarization, parahydrogen, ALTADENA, level anti-crossing, PHIP*

**ABSTRACT:** Level anti-crossings (LACs) are ubiquitous in quantum systems and have been exploited for spin order transfer in hyperpolarized nuclear magnetic resonance spectroscopy. This paper examines the manifestations of adiabatic passage through a specific type of LAC found in homonuclear systems of chemically inequivalent coupled protons incorporating parahydrogen ($pH_2$). Adiabatic passage through such a LAC is shown to elicit translation of the $pH_2$ spin order. As an example, with prospective applications in biomedicine, proton spin polarizations of at least 19.8±2.6% on the methylene protons and 68.7±0.5% on the vinylic protons of selectively deuterated allyl pyruvate ester are demonstrated experimentally. After ultrasonic spray injection of a precursor solution containing propargyl pyruvate and a dissolved Rh catalyst into a chamber pressurized with 99% para enriched $H_2$, the products are collected and transported to high magnetic field for NMR detection. The LAC-mediated hyperpolarization of the methylene protons is significant because of the stronger spin coupling to the pyruvate carbonyl $^{13}C$, setting up an ideal initial condition for subsequent coherence transfer by selective INEPT. Furthermore, the selective deuteration of the propargyl side-arm increases the efficiency and polarization level. LAC-mediated translation of parahydrogen spin order completes the first step toward a new and highly efficient route for $^{13}C$ NMR signal enhancement of pyruvate via side arm hydrogenation with parahydrogen.

## INTRODUCTION

Avoided crossings of eigenvalue curves, or level anti-crossings (LACs), are ubiquitous in quantum systems and underpin diverse physical phenomena.[1–5] For instance, LACs of spin states dressed by interaction with resonant radiofrequency (RF) fields provide a means to manipulate singlet-triplet imbalances,[6] and LACs induced by heteronuclear spin couplings have been extensively exploited for conversion of parahydrogen ($pH_2$) singlet order to $^{13}C$ magnetization at ultra-low magnetic fields,[7–14] thereby extending the applicability of parahydrogen enhanced NMR.[15–18] Apparently unnoticed until now is the significance of LACs in systems of chemically inequivalent protons incorporating $pH_2$ spin order. It will be shown here that adiabatic passage through such LACs can elicit translation of bilinear spin order to initially unpolarized protons in the molecule with an efficiency that depends on the spin couplings and relative proton isotropic chemical shifts. This quantum effect will enable a new and practical route to spin order transfer to $^{13}C$ for NMR signal enhancement of pyruvate and related $pH_2$ adducts with applications in biomedicine.[18–21]

## THEORY

The essential aspects of the spin dynamics are illustrated in a three-proton AMX spin system (Pople Notation[22]) formed by hydrogenation with $pH_2$, such as in the catalytic hydrogenation of a selectively deuterated propargyl ester to the allyl ester, as shown in Scheme 1.

**Scheme 1. Hydrogenation of selectively deuterated propargyl esters with parahydrogen.**

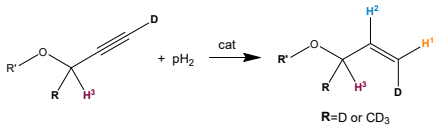


**R**=D or $CD_3$

Protons $H^1$ and $H^2$ are assumed to originate from $pH_2$, and $H^3$ is an initially unpolarized proton – e.g., the allyl methylene proton. The importance of the two different R groups in scheme 1 derives from the perturbation on the isotropic chemical shifts $\delta_i$ of the three protons: for R=D, $\delta_2 > \delta_1 > \delta_3$, while for R=$CD_3$, $\delta_2 > \delta_3 > \delta_1$. For the present purposes, the spin couplings to $^2H$ and nuclei in the R′ group are unimportant and will be ignored. The isotropic spin Hamiltonian pertinent to non-viscous solutions has the form

$$\hat{H}(B) = \sum_{i<j}^{3} J_{ij}\hat{\mathbf{I}}_i \cdot \hat{\mathbf{I}}_j + \sum_{i=1}^{3} \gamma B(1-\delta_i)\hat{I}_{zi} \qquad (1)$$

where $\gamma$ is the proton gyromagnetic ratio, $B$ is the applied static magnetic field, $\hat{I}_{zi}$ is the z-component of the $i^{th}$ spin operator $\hat{\mathbf{I}}_\mathbf{i}$, and $J_{ij}\hat{\mathbf{I}}_i \cdot \hat{\mathbf{I}}_j$ is the isotropic spin-spin coupling between protons $H^i$ and $H^j$. For the analytical treatment, we assume idealized Hamiltonians with

$$|J_{12}| \gg |J_{23}| \text{ and } J_{13} = 0,$$

and we consider three different constructs for an AMX spin system, designated C1, C2 and C3, defined in Table 1. The three constructs differ only in the relative order of the isotropic chemical shifts.

At the instant of hydrogenation, the projection operator for the $pH_2$ singlet state is

$$\hat{\rho}_s = \frac{1}{4}(|S_0\alpha\rangle\langle S_0\alpha| + |S_0\beta\rangle\langle S_0\beta|)$$

$$= \left(\frac{\hat{1}}{4} - \hat{\mathbf{I}}_1 \cdot \hat{\mathbf{I}}_2\right) \otimes \frac{1}{2}\hat{1} \qquad (2)$$

If $|J_{12}| \gg |J_{23}|$, then at a sufficiently low magnetic field $B_{low}$ the commutator $\left[\hat{H}(B_{low}), \hat{\rho}_s\right] \approx 0$, and the singlet order will remain essentially intact after averaging over the kinetic time distribution of individual hydrogenation events, and the time-averaged density operator for the ensemble of hydrogenation adducts will be $\langle\hat{\rho}_s\rangle \approx \hat{\rho}_s$. In the ALTADENA (Adiabatic Longitudinal Transport After Dissociation Engenders Net Alignment) effect,[2,3] the hydrogenation adducts formed at $B_{low} \approx 0$ are adiabatically transported to high magnetic field where weak coupling prevails and the NMR spectrum is acquired. Adiabatic passage, where individual spin states evolve without a change in their occupancy, occurs when the change in the spin Hamiltonian is sufficiently slow to avoid stimulating transitions between eigenstates, yet fast enough to avert significant spin relaxation.[5,13] Under such conditions, the density operator resulting from adiabatic transport over a time $\tau_{tr}$ that is short compared to the spin-lattice relaxation times can be approximated by unitary evolution:

$$\hat{\rho}_f(\tau_{tr}) = \hat{U}(\tau_{tr})\langle\hat{\rho}_s\rangle\,\hat{U}^{-1}(\tau_{tr}) \qquad (3)$$

where $\hat{U}(\tau_{tr}) = \exp\left(-i\int_0^{\tau_{tr}} dt'^{\hat{H}(t')}\right)$.

In the arrow notation, this transformation is expressed as $\langle\hat{\rho}_s\rangle \xrightarrow{\hat{H}(B)} \hat{\rho}_f$. In the trivial case where $J_{23} \to 0$ and $J_{13} \to 0$, $H^3$ is isolated, and the density operator $\hat{\rho}_f$ is like that of the original ALTADENA effect for two weakly coupled protons[2,3]:

$$\left(\frac{\hat{1}}{4} - \hat{\mathbf{I}}_1 \cdot \hat{\mathbf{I}}_2\right) \otimes \frac{1}{2}\hat{1} \xrightarrow{\hat{H}(B(t)),\ adiabatic}$$

$$\frac{\hat{1}}{8} - \frac{1}{2}\hat{I}_{z1}\hat{I}_{z2} \pm \frac{1}{4}\left(\hat{I}_{z1} - \hat{I}_{z2}\right) \qquad (4)$$

The sign of the third term in Eq. (4) depends on the relative signs of $J_{12}$ and $\delta_1 - \delta_2$.

Rotating frame eigenvalue correlation diagrams for the C1 and C3 type constructs are shown at the top of Fig. 1. A LAC is apparent for C1, but not for C3 where $\delta_3$ is bracketed by $\delta_1$ and $\delta_2$. The initial and final state populations resulting from adiabatic passage are indicated by the blue disks, and the hyperpolarized single-quantum NMR transitions involving each of the three protons in the weak-coupling regime are indicated by the color-coded arrows. Because there is no LAC for C3, the transitions of $H^3$ are unpolarized. In contrast, when $\delta_3$ lies outside the range spanned by $\delta_1$ and $\delta_2$ (either above or below) as in C1 or C2, the transitions of $H^3$ are hyperpolarized (burgundy dashed arrows).

The corresponding analytical calculations of the final density operator $\hat{\rho}_f$ resulting from unitary adiabatic propagation from the strong to weak coupling regimes for the idealized constructs C1, C2, and C3, according to Eq. (3), are reported in Table 1.

**Table 1. Density operators resulting from adiabatic passage from strong to weak coupling of idealized AMX spin systems, assuming $J_{12} \gg J_{23}$ and $J_{13} = 0$.**

| Construct | Hamiltonian parameters | LAC? | Final Density Operator, $\hat{\boldsymbol{\rho}}_\mathbf{f}$ |
|---|---|---|---|
| C1 | $\delta_2 > \delta_1 > \delta_3$ or $\delta_3 > \delta_1 > \delta_2$ | YES | $\frac{\hat{1}}{8} - \frac{1}{2}\hat{I}_{z2}\hat{I}_{z3} \pm \frac{1}{4}\left(\hat{I}_{z2} - \hat{I}_{z3}\right)$ |
| C2 | $\delta_1 > \delta_2 > \delta_3$ or $\delta_3 > \delta_2 > \delta_1$ | YES | $\frac{\hat{1}}{8} - \frac{1}{2}\hat{I}_{z1}\hat{I}_{z3} \pm \frac{1}{4}\left(\hat{I}_{z1} - \hat{I}_{z3}\right)$ |
| C3 | $\delta_2 > \delta_3 > \delta_1$ or $\delta_1 > \delta_3 > \delta_2$ | NO | $\frac{\hat{1}}{8} - \frac{1}{2}\hat{I}_{z1}\hat{I}_{z2} \pm \frac{1}{4}\left(\hat{I}_{z1} - \hat{I}_{z2}\right)$ |

For C1 and C2, the final density operators are identical in form to Eq. (4) but with proton labels 1 and 3 or 2 and 3 interchanged, respectively. For C3, $\hat{\rho}_f$ is the same as in Eq (4). The quantity $\langle\hat{I}_{z3}\rangle = Tr\left(\hat{I}_{z3} \cdot \hat{\rho}_f\right)$ provides a measure of the efficiency of the conversion of scalar $pH_2$ spin order (Eq. 1) into $H^3$ polarization. As seen in Tables 1 and 2, adiabatic passage through the LAC results in spin exchange involving both the linear and bilinear terms of $\hat{\rho}_f$, leading to the complete transfer of parahydrogen-derived spin order to the initially unpolarized proton in the molecule. The density operator calculations confirm that when the chemical shift of $H^3$ is intermediate to those of $H^1$ and $H^2$, $H^3$ remains unpolarized, irrespective of $J_{23}$.

Let us now consider the implications of the LAC-mediated proton spin-exchange of parahydrogen spin order for producing $^{13}C$ hyperpolarization in pyruvate and other carboxylic acids. While pyruvate is not directly producible by hydrogenation, attachment of the propargyl side-arm provides an unsaturated bond for addition of $pH_2$,[24] as in Scheme 1. In this side-arm hydrogenation (SAH) methodology, the $pH_2$ spin order needs to be transferred across the ester linkage to the carbonyl $^{13}C$, and then the side-arm is removed by hydrolysis to afford pyruvate. Propargylic side-arms offer greater chemical stability and higher rates of hydrogenation[7,25] than vinylic side-arms.

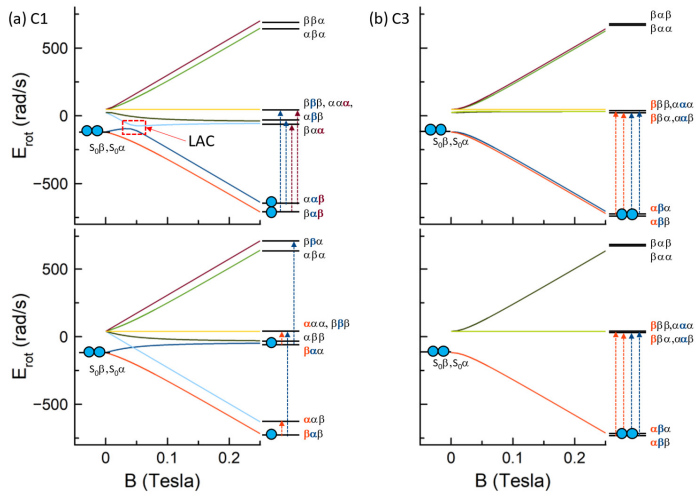


Figure 1. Rotating frame eigenvalue correlation diagrams for model Hamiltonians of type C1 and C3 as a function of the static magnetic field with $\bar{J}_{12} = 25$ Hz and $\bar{J}_{23} = 5$ Hz (upper diagrams) or $\bar{J}_{23} = 0$ Hz (lower diagrams). (a) C1, $\{\delta_1, \delta_2, \delta_3\}$ ={0,+10,-10} ppm. (b) C3, $\{\delta_1, \delta_2, \delta_3\} = \{+10,-10, 0\}$ ppm. The LAC is seen in the dashed red box. Orange, blue, and burgundy arrows indicate polarized single spin transitions of $H^1$, $H^2$ and $H^3$, respectively. In the absence of a LAC, transitions of $H^3$ remain unpolarized. The correlation diagram for C2 is analogous to C1. Curves were calculated using the SpinDynamica package[26] in Wolfram's Mathematica.

Disadvantageously, the $pH_2$ proton pair in allyl ester adducts is further away from the $^{13}C$ target due to the intervening $CH_2$ group in the former, and the spin-spin couplings to the nearest pyruvate $^{13}C$ are too small to mediate efficient coherence transfer in a single step.[27] This motivated the development of various two-step relayed coherence transfer pulse sequences[25,28–30] that operate on PASADENA-derived $\hat{I}_{z1}\hat{I}_{z2}$ spin order generated at high magnetic field.[15,16] Advantageously, LAC mediated translation to the $H^3$ (methylene) proton(s) in allyl ester sidearms of type C1 is significant because of the stronger spin coupling to the pyruvate carbonyl $^{13}C$, setting up an ideal initial condition for subsequent coherence transfer to the carbonyl $^{13}C$ by selective INEPT.[31]

The spin polarizations after adiabatic transport were evaluated for several pyruvate esters of interest (scheme 2) by numerical density matrix simulations and are reported in Table 3. Firstly, the results confirm the importance of the relative ordering of the chemical shifts (and hence the Zeeman energies) of the two $pH_2$ sourced protons and the relay proton(s). While (*Z*)-allyl-3-*d* 2-oxopropanoate-1-$^{13}C$ (APd) is a type C1 molecule, 3-$d_3$-1-d-buten-2-yl ($BPd_4$)[32] has the chemical shift ordering of C3 and *is thus predicted to not exhibit a LAC*. Even though APd and $BPd_4$ differ only in the attachment of a -$CD_3$ group at the methylene carbon, the methylation has had the effect of changing the chemical shift ordering, thus switching-off the LAC-mediated spin exchange process.

Secondly, the results in Table 3 show that selective deuteration can increase the efficiency of symmetry breaking conversion of $pH_2$ spin order into NMR-observable Zeeman order.[7,29] In non-deuterated AP or BP, J couplings to $H^5$ incur substantial irreversible loss of $pH_2$ spin order upon hydrogenation. Because $J_{25} > J_{12}, J_{23}$, there is a large admixture of the $H^5$ spin-state in the low field eigenstates of the adduct. The destructive effect of $J_{25}$ in the non-deuterated form is evident by evaluating $Tr\{\hat{\rho}_s \cdot \langle\hat{\rho}_s\rangle\}$. Recall that for a pure state, $Tr\{\hat{\rho}^2\} = 1$, but since $H^3$ and $H^5$ are initially unpolarized, $Tr\{\hat{\rho}^2\} = 1/4$ maximally. If $J_{15} \to 0$, one obtains $Tr\{\hat{\rho}_s \cdot \langle\hat{\rho}_s\rangle\}$=0.21, but if $\bar{J}_{15} = 17.2$ Hz (as in AP), $Tr\{\hat{\rho}_s \cdot \langle\hat{\rho}_s\rangle\}$=0.122. The loss can be mitigated by selective deuteration at $H^5$, since $J_{HD}/J_{HH} \approx 1/7$.

**Scheme 2. Molecular embodiments under study**

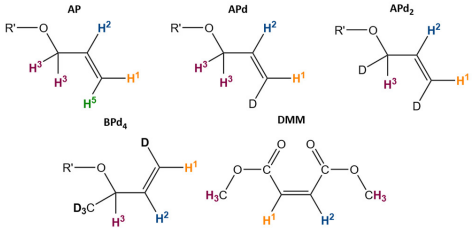


AP = allyl 2-oxopropanoate-1-$^{13}C$; APd = (*Z*)-allyl-3-*d* 2-oxopropanoate-1-$^{13}C$, $APd_2$ = (Z)-allyl-1,3-*d* 2-oxopropanoate-1-$^{13}C$; DMM = dimethyl maleate.

**Table 2. Zeeman order produced by adiabatic passage from strong to weak coupling for idealized constructs**

| Hamiltonian | $J_{23}=0$ | | | $J_{23}>0$ | | |
|---|---|---|---|---|---|---|
| Chemical Shifts | $\langle I_{1z}\rangle$ | $\langle I_{2z}\rangle$ | $\langle I_{3z}\rangle$ | $\langle I_{1z}\rangle$ | $\langle I_{2z}\rangle$ | $\langle I_{3z}\rangle$ |
| C1 $\delta_2>\delta_1>\delta_3$ | $\frac{1}{2}$ | $-\frac{1}{2}$ | 0 | 0 | $\frac{1}{2}$ | $-\frac{1}{2}^{a}$ |
| C3 $\delta_2>\delta_3>\delta_1$ | $\frac{1}{2}$ | $-\frac{1}{2}$ | 0 | $\frac{1}{2}$ | $-\frac{1}{2}$ | 0 |
| C4 $\delta_1=\delta_2 \neq \delta_3=\delta_4$ | 0 | 0 | 0 | $\frac{1}{4}$ | $\frac{1}{4}$ | $-\frac{1}{2}^{b}$ |

a. $\sum\langle I_z\rangle$ over both methylene relay protons in AP and APd. b. $\sum\langle I_z\rangle$ over all methyl protons.

**Table 3. Numerical simulations of Zeeman order produced in the molecular embodiments**

| Construct | Molecule | $\langle I_{1z}\rangle$ | $\langle I_{2z}\rangle$ | $\langle I_{3z}\rangle$ |
|---|---|---|---|---|
| C1 | AP | -.095 | +.28 | -.27[a] |
| | APd, $APd_2$ | -.0028 | +.42 | -.42[a] |
| C3 | $BPd_4$ | -.46 | +.46 | .0024 |
| C4 | DMM | 0.24 | 0.24 | -0.48[b] |

Moreover, if hydrogenation is performed in a small but finite magnetic field (e.g., Earth's field) where deuterons and protons are only weakly coupled, losses due to state mixing are negligible. The numerical simulation results in Table 3, calculated assuming perfect adiabatic passage, show that deuteration at $H^5$ affords a ~50% increase of $\langle I_{3z}\rangle$ after adiabatic passage through the LAC. The theoretical maximum achievable polarization of $H^3$, neglecting spin relaxation, is 84% in $APd_2$ (in APd, the polarization is divided equally between the two methylene protons). Simulation details and MATLAB/Spinach source code are provided in the Supporting Information.

## EXPERIMENTAL

The LAC-mediated proton spin exchange in AP and APd (after their formation by Rh catalyzed hydrogenation with $pH_2$ at 2.4 mT) was studied with the apparatus diagrammed in Fig. 2(a). A $d_6$-acetone solution of the alkyne precursor and dissolved Rh catalyst was infused through an ultrasonically vibrated nozzle into a funnel shaped reaction chamber pressurized to 6 bars with 99% enriched $pH_2$. Experiments were performed with a fixed 4:1 substrate:catalyst ratio with either 2 mM or 10 mM Rh(cod)(dppb)$BF_4$ catalyst concentration. Immediately after collecting 0.5 mL of the $pH_2$ adduct solution, the liquid was drawn into the Varian 400 MHz flow NMR probe at precisely controlled withdrawal rates varying from 0.2 to 5 mL/min, corresponding to transport times of $\tau_{tr}=100$ to 4 $s$, respectively, using a Chemyx™ 4000 dual syringe pump. The high-resolution $^1H$ NMR spectra were acquired on a Varian VNMRS spectrometer with a 2.25 $\mu s$ 90° flip-angle pulse. This choice of flip-angle suppresses the bilinear operator terms in $\hat{\rho}_f$ as well as the possible PASADENA signals stemming from any ongoing hydrogenation after transport to high magnetic field. Complete experimental details, including the synthesis of the isotopically labelled propargyl pyruvate and acetate substrates, are provided in the Supporting Information.

Fig. 2(b) plots the numerically simulated spin polarization, $P_i=2\langle\hat{I}_{zi}\rangle$, of each proton in $APd_2$ as a function of flow rate. These simulations indicate that in our system we can expect to approach the adiabatic regime at flow rates slower than about 2 mL/min ($\tau_{tr}>10\ s$), which is easily accessible by our syringe pump, probe, and fluid handling system. The polarization of the $H^2$ proton is expected to be invariant of the flow rate. However, it is important to note that these simulations do not account for the spin-lattice relaxation during transport.T High field inversion-recovery $T_1$ measurements on thermally polarized APd reaction products (with catalyst present) indicate that the $H^3$ $T_1$ is significantly shorter at 6.4 $s$ compared to the 9.2 $s$ and 9.6 $s$ relaxation times of the $H^1$ or $H^2$ protons, respectively (see Supporting Information).

## RESULTS AND DISCUSSION

The 400 MHz $^1H$ ALTADENA NMR spectra of AP and APd acquired after ultrasonic spray injection of the propargyl pyruvate precursor solutions containing 2 mM Rh catalyst into the reaction chamber pressurized with 99% $pH_2$ followed by infusion into the NMR flow probe at 3 mL/min ($\tau_{tr}$=6.6 s) are presented in Fig. 3(a,b). Superimposed on these spectra are the corresponding numerical simulations based on the measured magnetic field profile of the 9.4 T Bruker Ultrashield magnet. Each spectrum has been normalized to its $H^2$ peak amplitude. Without any fitting parameters, excellent agreement between theory and experiment is obtained except for the $H^3$ resonance, which is noticeably lower in intensity than in the simulated spectra of both AP and APd. The discrepancy is attributed to the shorter spin-lattice relaxation time of the $H^3$ methylene protons (see Supporting Information). The effects of differential spin-lattice relaxation losses during transport become even more pronounced at lower flow rates (see Supporting Information). Fig. 3(c) presents the spectrum obtained using the same flow rate of 3 mL/min but with a 5x more concentrated precursor solution (10 mM Rh and 40 mM AP or APd). For APd, a LAC mediated polarization of $P_3$ = 19.8 ± 2.6% was obtained for the initially unpolarized relay (methylene) protons, while a remarkable $P_2$=68.7 ± 0.5% polarization (averaged over 3 trials) was obtained for the vinylic $H^2$ proton originating from $pH_2$. Interestingly, the $H^1$ signal in the spectrum of APd obtained using the more concentrated precursor solution exhibits a clear antiphase doublet that defied numerical simulation. This contrasts with the net emission doublet observed with the APd precursor solution of lower concentration (Fig. 3b), consistent with theory. Signal enhancement and polarization values were calculated using the signals in the thermally polarized spectra shown in Fig. 3(d) and are reported in Table S1 of the Supporting Information.

**Commented [LMP1]:** Needs to be centered

**Commented [FJ2]:** Does this "a" and "b" in Table 3 need to specified as it is in Table 2?

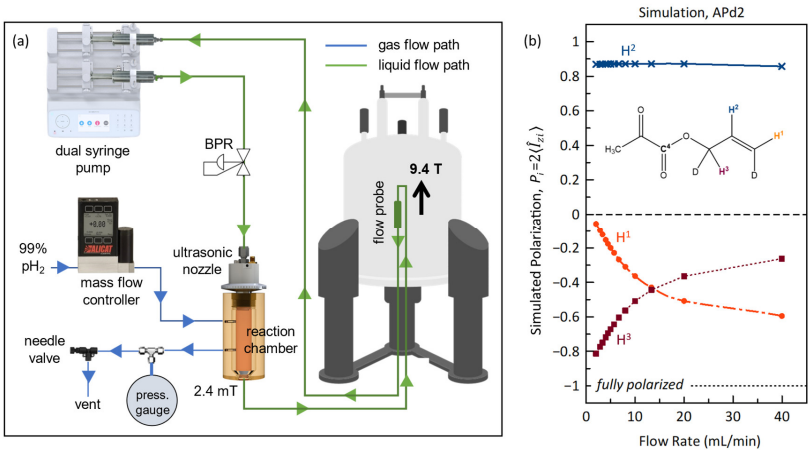


Figure 2. (a) Block diagram of the ultrasonic spray-injection reactor system interfaced to the flow NMR spectrometer. The tubing connecting the withdrawal syringe to the reaction chamber outlet, including the 60 $\mu$L flow cell, is initially prefilled with solvent and the reaction chamber pressurized with 6 bars 99% $pH_2$. The precursor solution is infused through an ultrasonic nozzle (3.5 W, 120 kHz) into the chamber at a flow rate of 5 mL/min. Products accumulate at the bottom of the funnel shaped chamber and are drawn into the NMR probe at precisely controlled syringe pump flow rates. BPR = back-pressure regulator (5.17 bars). Further details are provided in the Supporting Information. (b) Numerical density matrix calculations of the spin polarization (neglecting spin relaxation) of individual protons in $APd_2$ as a function of the syringe pump withdrawal rate, estimated from the transport time $\tau_{tr}$ used in the simulation, the volume (0.33 mL), and the measured field profile of the Bruker 9.4 T Ultrashield magnet along the flow trajectory. Spin polarizations were computed using Spinach.[32]

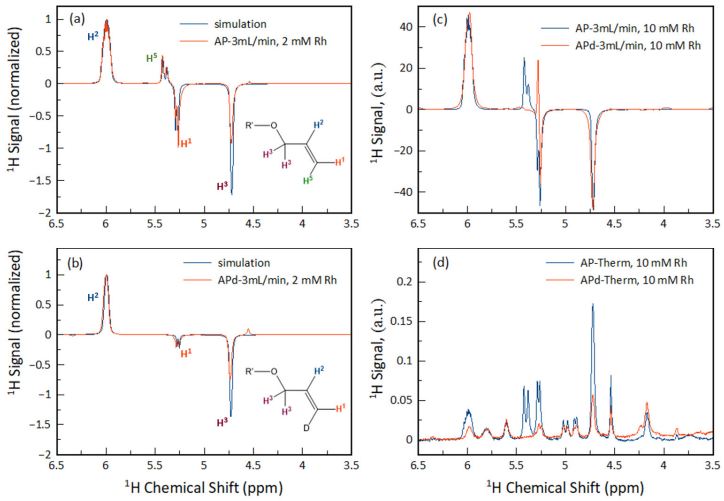


Figure 3. (a,b) 400 MHz $^1$H ALTADENA experimental spectra (in red) and numerically simulated $^1$H ALTADENA spectra (in blue) of AP and APd, respectively, obtained by hydrogenation of 8 mM propargyl pyruvate precursors with $pH_2$ using 2 mM Rh catalyst in the 2.4 mT fringe field followed by transport into the flow probe at a flow rate of 3 mL/min for detection at 9.4 T using a 90° RF pulse. The spectra have been normalized to the $H^2$ peak. (c) 400 MHz $^1$H ALTADENA spectra of AP (in blue) and APd (in red) obtained by hydrogenation as in (a,b) but with 40 mM propargyl pyruvate precursors and 10 mM Rh catalyst. The $H^2$ peak in the spectrum of AP has been scaled to match the $H^2$ peak of the APd spectrum. (d) Thermally polarized spectra of the reaction product solutions of (c), acquired by accumulation of 4 transients, and plotted on the same vertical axis as (c).

Closely related to the LAC-mediated spin exchange in AMX spin systems is the net alignment spin order produced in $C_s$-symmetric AA'XX' adducts of $pH_2$. The archetypical example is dimethyl maleate (DMM), a system addressed in several previous accounts[33,34] prior to the understanding of the role of LACs in ALTADENA experiments.[35] For completeness, the analytical form of the density operator for the associated idealized construct C4, defined in Table 2, and a numerical spectral simulation for the DMM embodiment, are provided in the Supporting Information.

## CONCLUSION

In summary, parahydrogen induced hyperpolarization levels of up to 19.8% (and 68.7% on the $H^2$ proton) on the methylene relay protons ($H^3$) of (*Z*)-allyl-3-*d* 2-oxopropanoate-1-$^{13}$C (APd) were demonstrated using the LAC-mediated proton spin-exchange method introduced herein. Such high polarization levels are remarkable considering the relatively short relaxation time of these protons ($T_1$ = 6.4 s). Even higher polarization levels might be achieved by reducing $T_1$ losses during adiabatic transport as may be realized using a variable syringe pump flow rate to maintain the constant-adiabaticity[13] criterion, or by employing a bench-top NMR spectrometer with a reduced flow path length. A further increase in the $H^3$ proton polarization level is anticipated in (Z)-allyl-1,3-*d* 2-oxopropanoate-1-$^{13}$C ($APd_2$) adducts where the spin-lattice relaxation time is likely to be increased by replacement of the -$CH_2$- with -CHD- on the allyl side-arm. An important implication of these results is that LAC-mediated proton spin-exchange of $pH_2$ spin order in the AMX spin systems completes the first step toward spin order transfer to $^{13}$C in pyruvate and other key metabolites. The deuteration pattern in $APd_2$ also lends itself to a higher efficiency (by a factor of 2) in the selective coherence transfer from $H^3$ to the pyruvate carbonyl $^{13}$C,[7,36,37] providing an overall maximum theoretical efficiency of 84% for the conversion of $pH_2$ spin order to $^{13}$C magnetization on the metabolite. This is similar to the theoretical maximum efficiency of the high-field relayed-coherence transfer RF pulse sequences based on high-field $pH_2$ addition to propargyl side-arms as well as the slower reacting and less stable vinyl ester side-arms (which lack relay protons). Advantageously, the proposed LAC-INEPT approach requires only a single coherence transfer step, thereby reducing $T_2$ decoherence losses. Moreover, the approach is compatible with hydrogenation in a high-performance hydrogenation reactor (such as our ultrasonic spray injection system) operating outside of the NMR magnet. Polarization levels achievable by our LAC-INEPT approach are competitive with the best results obtained by dissolution DNP,[19,38] but with substantially lower cost, higher reproducibility, shorter polarization times, and perhaps most importantly, compatibility with continuous-flow chemistry and separations.

## ASSOCIATED CONTENT

**Supporting Information**. The Supporting Information document provides details of the experimental instrumentation, protocols, synthesis and characterization of isotopically labelled compounds, equations used to evaluate signal enhancements and spin polarizations, spin interaction parameters for the studied molecules, analytical derivation details, Mathematica/SpinDynamica source code, Spinach/Matlab source code, and additional spectral simulations. This material is available free of charge via the Internet at http://pubs.acs.org.

## AUTHOR INFORMATION

### Corresponding Author

*Clifford R. Bowers, 2001 Museum Road, University of Florida, Gainesville, Florida 32611 USA, email: bowers@chem.ufl.edu.

## ACKNOWLEDGMENT

This work was supported by NSF grants CHE-2108306, CBET-1933723, and the National High Magnetic Field Laboratory User Collaborative Grants Program, which is supported by NSF DMR-1644779 and the State of Florida. AG and VMD thank the National Institutes of Health, grants R35GM137893-01 and R35GM127071, respectively.

## REFERENCES

(1) Zhou, J.; Huang, P.; Zhang, Q.; Wang, Z.; Tan, T.; Xu, X.; Shi, F.; Rong, X.; Ashhab, S.; Du, J. Observation of Time-Domain Rabi Oscillations in the Landau-Zener Regime with a Single Electronic Spin. *Phys Rev Lett* **2014**, *112* (1), 010503. https://doi.org/10.1103/PhysRevLett.112.010503.

(2) Rubbmark, J. R.; Kash, M. M.; Littman, M. G.; Kleppner, D. Dynamical Effects at Avoided Level Crossings: A Study of the Landau-Zener Effect Using Rydberg Atoms. *Phys Rev A (Coll Park)* **1981**, *23* (6), 3107–3117. https://doi.org/10.1103/PHYSREVA.23.3107.

(3) Non-Adiabatic Crossing of Energy Levels. *Proceedings of the Royal Society of London. Series A, Containing Papers of a Mathematical and Physical Character* **1932**, *137* (833), 696–702. https://doi.org/10.1098/RSPA.1932.0165.

(4) Corzilius, B. High-Field Dynamic Nuclear Polarization. *Annu Rev Phys Chem* **2020**, *71* (1), 143–170. https://doi.org/10.1146/annurev-physchem-071119-040222.

(5) Ivanov, K. L.; Pravdivtsev, A. N.; Yurkovskaya, A. v.; Vieth, H. M.; Kaptein, R. The Role of Level Anti-Crossings in Nuclear Spin Hyperpolarization. *Prog Nucl Magn Reson Spectrosc* **2014**, *81*, 1–36. https://doi.org/10.1016/j.pnmrs.2014.06.001.

(6) DeVience, S. J.; Walsworth, R. L.; Rosen, M. S. Preparation of Nuclear Spin Singlet States Using Spin-Lock Induced Crossing. *Phys Rev Lett* **2013**, *111* (17), 173002.

(7) Marshall, A.; Salhov, A.; Gierse, M.; Müller, C.; Keim, M.; Lucas, S.; Parker, A.; Scheuer, J.; Vassiliou, C.; Neumann, P.; Jelezko, F.; Retzker, A.; Blanchard, J. W.; Schwartz, I.; Knecht, S. Radio-Frequency Sweeps at {\mu}T Fields for Parahydrogen-Induced Polarization of Biomolecules. *arXiv* **2022**, *May 31*. https://doi.org/10.48550/arxiv.2205.15709.

(8) Goldman, M.; Jóhannesson, H. Conversion of a Proton Pair Para Order into 13C Polarization by Rf Irradiation, for Use in MRI. *C R Phys* **2005**, *6* (4–5), 575–581. https://doi.org/10.1016/J.CRHY.2005.03.002.

(9) Ripka, B.; Eills, J.; Kouřilová, H.; Leutzsch, M.; Levitt, M. H.; Münnemann, K. Hyperpolarized Fumarate via Parahydrogen. *Chemical Communications* **2018**, *54* (86), 12246–12249. https://doi.org/10.1039/c8cc06636a.

(10) N. Pravdivtsev, A.; v. Yurkovskaya, A.; N. Lukzen, N.; L. Ivanov, K.; Vieth, H.-M. Highly Efficient Polarization of Spin-1/2 Insensitive NMR Nuclei by Adiabatic Passage through Level Anticrossings. *J Phys Chem Lett* **2014**, *5* (19), 3421–3426. https://doi.org/10.1021/jz501754j.

(11) Jóhannesson, H.; Axelsson, O.; Karlsson, M. Transfer of Para-Hydrogen Spin Order into Polarization by Diabatic Field Cy-

cling. *C R Phys* **2004**, *5* (3), 315–324. https://doi.org/10.1016/J.CRHY.2004.02.001.
(12) Joalland, B.; Schmidt, A. B.; Kabir, M. S. H.; Chukanov, N. v.; Kovtunov, K. v.; Koptyug, I. v.; Hennig, J.; Hövener, J.-B.; Chekmenev, E. Y. Pulse-Programmable Magnetic Field Sweeping of Parahydrogen-Induced Polarization by Side Arm Hydrogenation. *Anal Chem* **2020**, *92* (1), 1340–1345. https://doi.org/10.1021/acs.analchem.9b04501.
(13) Rodin, B. A.; Eills, J.; Picazo-Frutos, R.; Sheberstov, K. F.; Budker, D.; Ivanov, K. L. Constant-Adiabaticity Ultralow Magnetic Field Manipulations of Parahydrogen-Induced Polarization: Application to an AA′X Spin System. *Physical Chemistry Chemical Physics* **2021**, *23* (12), 7125–7134. https://doi.org/10.1039/D0CP06581A.
(14) Knecht, S.; Blanchard, J. W.; Barskiy, D.; Cavallari, E.; Dagys, L.; van Dyke, E.; Tsukanov, M.; Bliemel, B.; Münnemann, K.; Aime, S.; Reineri, F.; Levitt, M. H.; Buntkowsky, G.; Pines, A.; Blümler, P.; Budker, D.; Eills, J. Rapid Hyperpolarization and Purification of the Metabolite Fumarate in Aqueous Solution. *Proceedings of the National Academy of Sciences of the United States of America* **2021**, *118* (13), e2025383118. https://doi.org/10.1073/pnas.2025383118.
(15) Bowers, C. R.; Weitekamp, D. P. Transformation of Symmetrization Order to Nuclear-Spin Magnetization by Chemical Reaction and Nuclear Magnetic Resonance. *Physical Review Letters* **1986**, *57* (21), 2645–2648. https://doi.org/10.1103/PhysRevLett.57.2645.
(16) Bowers, C. R.; Weitekamp, D. P. Parahydrogen and Synthesis Allow Dramatically Enhanced Nuclear Alignment. *Journal of the American Chemical Society* **1987**, *109* (18), 5541–5542. https://doi.org/10.1021/ja00252a049.
(17) Schmidt, A. B.; Hövener, J. B.; Bowers, C. R.; Buckenmaier, K.; Chekmenev, E. Y.; de Maissin, H.; Eills, J.; Ellermann, F.; Glöggler, S.; Gordon, J. W.; Knecht, S.; Koptyug, I. v.; Kuhn, J.; Pravdivtsev, A. N.; Reineri, F.; Theis, T.; Them, K. Instrumentation for Hydrogenative Parahydrogen-Based Hyperpolarization Techniques. *Analytical Chemistry* **2022**, *94* (1), 479–502. https://doi.org/10.1021/acs.analchem.1c04863.
(18) Hovener, J. B.; Pravdivtsev, A. N.; Kidd, B.; Bowers, C. R.; Gloggler, S.; Kovtunov, K. v.; Plaumann, M.; Katz-Brull, R.; Buckenmaier, K.; Jerschow, A.; Reineri, F.; Theis, T.; Shchepin, R. v.; Wagner, S.; Bhattacharya, P.; Zacharias, N. M.; Chekmenev, E. Y. Parahydrogen-Based Hyperpolarization for Biomedicine. *Angewandte Chemie International Edition* **2018**, *57* (35), 11140–11162. https://doi.org/10.1002/anie.201711842.
(19) Ardenkjaer-Larsen, J. H. On the Present and Future of Dissolution-DNP. **2016**, *264*, 3–12. https://doi.org/10.1016/j.jmr.2016.01.015.
(20) Heiden, M. G. V.; Cantley, L. C.; Thompson, C. B. Understanding the Warburg Effect: The Metabolic Requirements of Cell Proliferation. *Science (1979)* **2009**, *324* (5930), 1029–1033. https://doi.org/10.1126/SCIENCE.1160809/ASSET/C00CA2CE-14F9-4352-AC43-7D1BB04B41D8/ASSETS/GRAPHIC/324_1029_F4.JPEG.
(21) Kurhanewicz, J.; Vigneron, D. B.; Brindle, K.; Chekmenev, E. Y.; Comment, A.; Cunningham, C. H.; DeBerardinis, R. J.; Green, G. G.; Leach, M. O.; Rajan, S. S.; Rizi, R. R.; Ross, B. D.; Warren, W. S.; Malloy, C. R. Analysis of Cancer Metabolism by Imaging Hyperpolarized Nuclei: Prospects for Translation to Clinical Research. *Neoplasia* **2011**, *13* (2), 81–97. https://doi.org/10.1593/neo.101102.
(22) Bernstein, H. J.; Pople, J. A.; Schneider, W. G. The Analysis of Nuclear Magnetic Resonance Spectra: I. System of Two and Three Nuclei. *Can J Chem* **1957**, *35* (1), 67–83. https://doi.org/10.1139/v57-011.
(23) Pravica, M. G.; Weitekamp, D. P. Net NMR Alignment by Adiabatic Transport of Parahydrogen Addition Products to High Magnetic Field. *Chem Phys Lett* **1988**, *145* (4), 255–258. https://doi.org/10.1016/0009-2614(88)80002-2.
(24) Reineri, F.; Boi, T.; Aime, S. ParaHydrogen Induced Polarization of 13C Carboxylate Resonance in Acetate and Pyruvate. *Nat Commun* **2015**, *6* (1), 5858. https://doi.org/10.1038/ncomms6858.
(25) Svyatova, A.; Kozinenko, V. P.; Chukanov, N. v; Burueva, D. B.; Chekmenev, E. Y.; Chen, Y.-W.; Hwang, D. W.; Kovtunov, K. v; Koptyug, I. v. PHIP Hyperpolarized [1-13C]Pyruvate and [1-13C]Acetate Esters via PH-INEPT Polarization Transfer Monitored by 13C NMR and MRI. *Sci Rep* **2021**, *11* (1), 5646. https://doi.org/10.1038/s41598-021-85136-2.
(26) Bengs, C.; Levitt, M. H. SpinDynamica: Symbolic and Numerical Magnetic Resonance in a Mathematica Environment. *Magnetic Resonance in Chemistry* **2018**, *56* (6), 374–414. https://doi.org/10.1002/MRC.4642.
(27) Stewart, N. J.; Kumeta, H.; Tomohiro, M.; Hashimoto, T.; Hatae, N.; Matsumoto, S. Long-Range Heteronuclear J-Coupling Constants in Esters: Implications for 13C Metabolic MRI by Side-Arm Parahydrogen-Induced Polarization. *Journal of Magnetic Resonance* **2018**, *296*, 85–92. https://doi.org/10.1016/J.JMR.2018.08.009.
(28) Korchak, S.; Yang, S.; Mamone, S.; Glöggler, S. Pulsed Magnetic Resonance to Signal-Enhance Metabolites within Seconds by Utilizing Para -Hydrogen. *ChemistryOpen* **2018**, *7* (5), 344–348. https://doi.org/10.1002/open.201800024.
(29) Dagys, L.; Jagtap, A. P.; Korchak, S.; Mamone, S.; Saul, P.; Levitt, M. H.; Glöggler, S. Nuclear Hyperpolarization of (1-13C)-Pyruvate in Aqueous Solution by Proton-Relayed Side-Arm Hydrogenation. *Analyst* **2021**, *146* (5), 1772–1778. https://doi.org/10.1039/D0AN02389B.
(30) Ding, Y.; Korchak, S.; Mamone, S.; Jagtap, A. P.; Stevanato, G.; Sternkopf, S.; Moll, D.; Schroeder, H.; Becker, S.; Fischer, A.; Gerhardt, E.; Outeiro, T. F.; Opazo, F.; Griesinger, C.; Glöggler, S. Rapidly Signal-Enhanced Metabolites for Atomic Scale Monitoring of Living Cells with Magnetic Resonance. *Chemistry - Methods* **2022**, e202200023. https://doi.org/10.1002/CMTD.202200023.
(31) Bax, A. Structure Determination and Spectral Assignment by Pulsed Polarization Transfer via Long-Range 1H⍰13C Couplings. *Journal of Magnetic Resonance (1969)* **1984**, *57* (2), 314–318. https://doi.org/10.1016/0022-2364(84)90133-1.
(32) Hogben, H. J.; Krzystyniak, M.; Charnock, G. T. P.; Hore, P. J.; Kuprov, I. Spinach – A Software Library for Simulation of Spin Dynamics in Large Spin Systems. *Journal of Magnetic Resonance* **2011**, *208* (2), 179–194. https://doi.org/10.1016/J.JMR.2010.11.008.
(33) Haake, M.; Barkemeyer, J.; Bargon, J. Symmetry Breakdown during Parahydrogen-Labeling of Symmetric Substrates : Proton Spin Polarization and Singlet/Triplet Mixing Due to 13C-Isotopes in Natural Abundance. *J Phys Chem* **2002**, *99* (49), 17539–17543. https://doi.org/10.1021/j100049a012.
(34) Aime, S.; Gobetto, R.; Canet, D. Longitudinal Nuclear Relaxation in an A 2 Spin System Initially Polarized through Para-Hydrogen. *J Am Chem Soc* **1998**, *120* (27), 6770–6773. https://doi.org/10.1021/ja973240w.
(35) Buljubasich, L.; Franzoni, M. B.; Spiess, H. W.; Münnemann, K. Level Anti-Crossings in ParaHydrogen Induced Polarization Experiments with Cs-Symmetric Molecules. *Journal of Magnetic Resonance* **2012**, *219*, 33–40. https://doi.org/10.1016/j.jmr.2012.03.020.
(36) Levitt, M. H. Symmetry Constraints on Spin Dynamics: Application to Hyperpolarized NMR. *Journal of Magnetic Resonance* **2016**, *262*, 91–99. https://doi.org/10.1016/J.JMR.2015.08.021.
(37) Nielsen, N. C.; Schulte-Herbrüggen, T.; Sørensen, O. W. Bounds on Spin Dynamics Tightened by Permutation Symmetry Application to Coherence Transfer in I2S and I3S Spin Systems. *Mol Phys* **1995**, *85* (6), 1205–1216. https://doi.org/10.1080/00268979500101771.
(38) Ardenkjaer-Larsen, J. H.; Fridlund, B.; Gram, A.; Hansson, G.; Hansson, L.; Lerche, M. H.; Servin, R.; Thaning, M.; Golman, K.

Increase in Signal-to-Noise Ratio of > 10,000 Times in Liquid-State NMR. *Proc Natl Acad Sci U S A* **2003**, *100* (18), 10158–10163. https://doi.org/10.1073/pnas.1733835100.

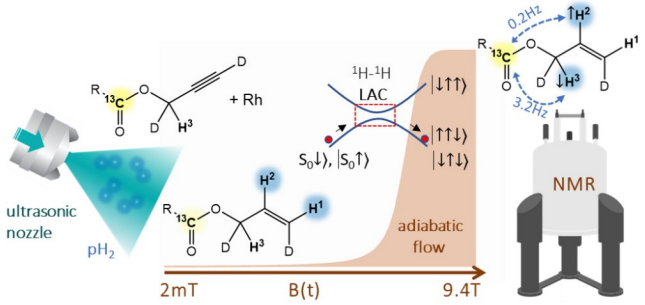
ultrasonic
nozzle
pH2
+ Rh
1H-1H
LAC
S0↓⟩, |S0↑⟩
|↓↑↑⟩
|↑↑↓⟩
|↓↑↓⟩
adiabatic
flow
2mT
B(t)
9.4T
0.2Hz
3.2Hz
NMR